Nanocarrier-Mediated Inhibition of Macrophage Migration Inhibitory Factor Attenuates Secondary Injury after Spinal Cord Injury

Tarun Saxena,[†] Kristin H. Loomis,[†] S. Balakrishna Pai,[†] Lohitash Karumbaiah,[‡] Eric Gaupp,[†] Ketki Patil,[†] Radhika Patkar,[†] and Ravi V. Bellamkonda*[,†]

[†]Wallace H. Coulter Department of Biomedical Engineering, Georgia Institute of Technology and Emory School of Medicine, Atlanta, Georgia 30332, United States and [‡]Regenerative Bioscience Center, The University of Georgia, Athens, Georgia 30602, United States

ABSTRACT Spinal cord injury (SCI) can lead to permanent motor and sensory deficits. Following the initial traumatic insult, secondary injury mechanisms characterized by persistent heightened inflammation are initiated and lead to continued and pervasive cell death and tissue damage. Anti-inflammatory drugs such as methylprednisolone (MP) used clinically have ambiguous benefits with debilitating side effects. Typically, these drugs are administered systemically at high doses, resulting in toxicity and paradoxically increased inflammation. Furthermore, these drugs have a small time window postinjury (few hours) during which they need to be infused to be effective. As an alternative to MP, we investigated the effect of a small molecule inhibitor (Chicago sky blue, CSB) of macrophage migration inhibitory factor (MIF) for treating SCI. The pleiotropic cytokine MIF is known to contribute to upregulation of several pro-inflammatory cytokines in various disease and injury states. *In vitro*, CSB administration alleviated endotoxin-mediated inflammation in primary microglia and macrophages. Nanocarriers such as liposomes can potentially alleviate systemic side effects of high-dose therapy by enabling site-specific drug delivery to the spinal cord. However, the therapeutic window of 100 nm scale nanoparticle localization to the spinal cord after contusion injury is not fully known. Thus, we first investigated the ability of nanocarriers of different sizes to localize to the injured spinal cord up to 2 weeks postinjury. Results from the study showed that nanocarriers as large as 200 nm in diameter could extravasate into the injured spinal cord up to 96 h postinjury. We then formulated nanocarriers (liposomes) encapsulating CSB and administered them intravenously 48 h postinjury, within the previously determined 96 h therapeutic window. *In vivo*, in this clinically relevant contusion injury model in rats, CSB administration led to preservation of vascular and white matter integrity, improved wound healing, and an increase in levels of arginase and other transcripts indicative of a resolution phase of wound healing. This study demonstrates the potential of MIF inhibition in SCI and the utility of nanocarrier-mediated drug delivery selectively to the injured cord.

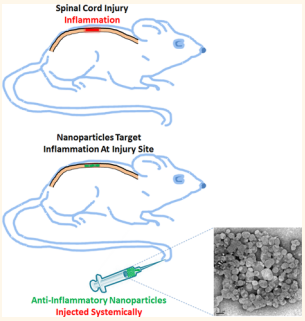

KEYWORDS: liposomes · nanoparticles · spinal cord injury · secondary injury · inflammation · macrophage migration inhibitory factor · Chicago sky blue

Injury to the spinal cord can result from acute compression, impact due to accidents, or lacerations due to knife and bullet wounds. While this primary trauma leads to immediate cell death and tissue damage, its sequelae initiate secondary injury, which can last from hours to weeks.[1,2] Secondary injury mechanisms are mediated in part by vascular changes such as reperfusion and hemorrhage, breakdown of the blood–spinal cord barrier (BSB), electrolyte imbalances such as increased intracellular calcium, biochemical changes such as excitotoxicity due to neurotransmitter accumulation as in glutamate excitotoxicity, and various other stimuli such as lipid peroxidation, free radical production, and edema.[3−5] A hallmark of secondary injury is heightened inflammation. This inflammation is largely mediated by resident glial cells (astrocytes and microglia) that become "activated" upon injury and also by incoming myeloid immune cells such as neutrophils and T-cells.[3,6,7] Activated glia and other infiltrating cells proliferate and produce both inflammatory and anti-inflammatory cytokines; however, the balance is skewed in favor of inflammatory cytokines and stimuli.[8−10] As time proceeds, over a few weeks, the activated glia and other infiltrating cells

* Address correspondence to ravi@gatech.edu.

Received for review October 20, 2014 and accepted January 14, 2015.

Published online January 14, 2015
10.1021/nn505980z

form a glial scar to wall off the injury site and prevent damage to the adjacent tissue.[1]

Inflammation due to secondary injury leads to continued cell death, demyelination, and tissue damage.[4] A critical intervention point in the treatment of SCI, therefore, is to stem the inflammation, as it is potentially preventable and/or reversible.[11] The current clinical treatment consists of using high-dose glucocorticoids such as methylprednisolone (MP). To be effective, MP has to be injected systemically at high doses within 8 h of SCI, with continued treatment over the next 24 h.[12−14] Treatment with MP has been controversial, and the high doses result in deleterious side effects. Thus, there are two immediate challenges in acute SCI treatment: to find alternatives to MP and to control inflammation *in situ*, at the site of SCI without inducing systemic side effects such as those from high-dose corticosteroid therapy.

Glucocorticoids such as MP can paradoxically increase inflammation by increasing the levels of migration inhibitory factor (MIF), a pro-inflammatory cytokine which is a key regulator of innate immunity.[15−17] MIF is rapidly released by immune cells and other cell types in the central nervous system upon exposure to inflammatory cytokines and, in general, counterregulates the action of glucocorticoids. Elevated levels of MIF have been observed in injured spinal cords acutely[18] and in the serum of human SCI patients chronically.[19] Because MIF modulates, directly or indirectly, the production of various pro-inflammatory cytokines such as interferon-γ (IFN-γ), tumor necrosis factor (TNF), the interleukins (IL) 2, 6, and 8, and several other cytokines and matrix metalloproteinases (MMPs),[17] all of which are implicated in secondary injury after SCI,[9] MIF inhibition is potentially an important target in SCI.[18,20−22] Furthermore, several small molecule inhibitors of MIF already exist,[23−25] thereby providing alternatives to glucocorticoids such as MP. In this study, we tested the potential of Chicago sky blue (CSB),[25] a potent allosteric inhibitor of MIF activity, as an anti-inflammatory drug. By noncovalently interacting with MIF protein trimers, a single molecule of CSB occupies the interface of two MIF trimers, leading to the loss of the pro-inflammatory activities of MIF and prevents MIF from binding to its receptor, CD74.[25] Additionally, CSB has also been shown to have antinociceptive effects in mice[26] and rescues neurons from glutamate excitotoxicity by competitively binding to glutamate receptors and preventing glutamate uptake.[26−28] *In vitro*, CSB is nontoxic to primary human fibroblasts at concentrations as high as 100 μM and has an IC_{50} that is at least 100 times lower than that of the prototypical MIF inhibitor ISO-1.[25]

Nanoparticle-based drug carriers are ideal candidates to modulate inflammation *in situ*, at the site of SCI without inducing systemic side effects such as those from high-dose corticosteroid therapy.[29,30] By engineering nanoparticles that have enhanced circulation times,[31,32] and taking advantage of the disrupted vasculature at the site of SCI,[3,33] the enhanced permeability and retention effect[34−36] can be leveraged to obtain site-specific drug delivery while reducing systemic drug levels.[37−40] Elucidating the therapeutic window after SCI during which nanoparticles can extravasate into the injured cord and how this "nanoparticle permeability" changes with nanoparticle size[41] can provide information about nanocarrier-based therapeutic intervention in SCI.

In this study, we assessed the anti-inflammatory properties of CSB *in vitro*. We then determined the time and size dependency of nanoparticle extravasation into the injured spinal cord. Finally, we designed poly(ethylene glycol) (PEG)-coated liposomal *stealth* nanocarriers of CSB and evaluated their effect *in vivo*, *via* intravenous injection 48 h postinjury. Additional investigations were carried out to assess the acute anti-inflammatory effects of CSB therapy to determine if nanocarrier-mediated CSB therapy was a viable therapeutic approach after SCI.

RESULTS

***In Vitro* Anti-inflammatory Activity of CSB.** In this study, we wanted to determine the anti-inflammatory effects of a recently discovered small molecule inhibitor of MIF, CSB. We hypothesized that MIF inhibition can be beneficial in mitigating secondary injury in SCI. To determine the toxicity of CSB, primary glial cells such as microglia and astrocytes and the murine macrophage cell line, RAW 264.7, were incubated with CSB for 24 h at a dose of 10 μM. Using a colorimetric assay to measure cell viability,[42] it was determined that CSB was nontoxic to both primary cells (Figure 1A) and cell lines at a concentration of 10 μM. We then assessed the anti-inflammatory activity of CSB in both primary cells and cell lines. To create an inflammatory environment, we activated the cells with lipopolysaccharide (LPS) after priming cells with IFN-γ.[43,44] This preparation is known to upregulate MIF, as well as other inflammatory cytokines such as TNF-α, which can further elevate MIF levels.[15,45] After treating cells overnight with LPS and IFN-γ, we treated cells with 10 μM CSB for 24 h, following which cells and cell media were collected for gene and protein analysis, respectively. Using a colorimetric assay (Griess assay[46]) for nitrite production (as MIF synergizes with cytokines to increase nitrite production[45]), we observed that CSB addition attenuated nitrite production in both primary cells and cell lines (Figure 1B). Furthermore, CSB addition reduced TNF-α production along with other inflammatory cytokines in these cells, as assessed by ELISA (Figure S1A,B, Supporting Information). Importantly, the addition of CSB alone did not lead to the upregulation of any inflammatory transcripts (Figure S1C, Supporting Information). Taken together, these data

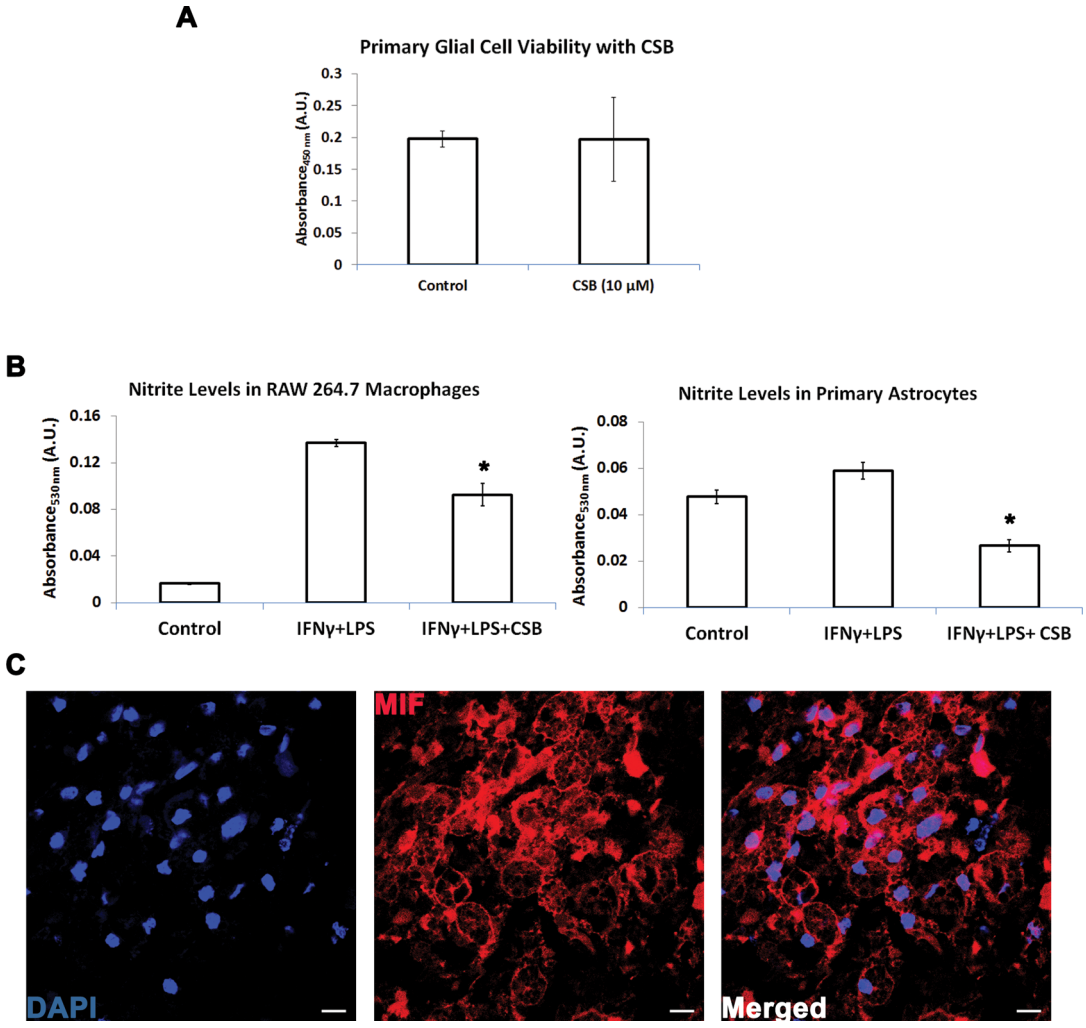

Figure 1. *In vitro* **cytotoxicity and anti-inflammatory activity of Chicago sky blue (CSB). (A) CSB is nontoxic to primary glial cells (mixed astrocyte and microglial cultures) at a concentration of 10 μM, after 24 h of incubation. CSB addition leads to decrease in nitrite levels in (B) RAW 264.7 macrophages and primary glial cells. Cells were activated by the addition of 10 ng/mL lipopolysaccharide in the presence or absence of 100 U/mL IFN-γ for 24 h, following which the cells were incubated with 1 mL of fresh medium with or without 10 μM CSB. Data are represented as mean $\pm$ SD, and means with *$p < 0.05$ are significantly different from the appropriate controls. (C) Micrograph showing that macrophage migration inhibitory factor (red) is present in SCI lesions in spinal cord sections obtained 96 h post-SCI. Cell nuclei are stained with DAPI (blue). Scale bar in (C) is 20 μm.**

demonstrate the anti-inflammatory potential of CSB *in vitro*.

Time and Size Dependency of Nanoparticle Extravasation Post-SCI. Adult male Sprague–Dawley rats were subjected to a clinically relevant contusion SCI at the thoracic-9 (T9) vertebral level using a force-controlled impaction device.[47] To determine the permeability of the injured spinal cord to nanoparticles as a function of time postinjury and as a function of nanoparticle size, we intravenously injected a nanoparticle cocktail comprising nanoparticles of three distinct sizes (40, 200, and 1000 nm) and fluorescent spectra at different times postinjury (48 h, 96 h, 1 week, and 2 weeks). These sizes of nanoparticles were chosen to span three different orders of magnitude in size. Equal amounts (by % solids)[41] of nanoparticles were injected at each of the indicated time points. These particles were chosen because they have long circulation times, similar to stealth liposomes, and allow for tight control over size with easy spectral detection. The particles were allowed to circulate for 6 h, after which the animals were thoroughly perfused and their spinal cords dissected and prepared for fluorescence microscopy. We observed that, at all time points, the 1000 nm particles never extravasated into the spinal cord parenchyma, although particles were observed circulating in the blood (data not shown). At both 48 h (Figure 2Ai) and 96 h (Figure 2Aii) postinjury, nanoparticles (40 and 200 nm) extravasated into the cord parenchyma at the injury epicenter and were located adjacent to the disrupted vasculature (as assessed by rat endothelial cell antigen staining). However, at 1 week (Figure 2Aiii) and 2 weeks (Figure 2Aiv) postinjury, very few particles were observed, and the particles observed were trapped within the blood vessels and could not extravasate into the spinal cord tissue. We further observed

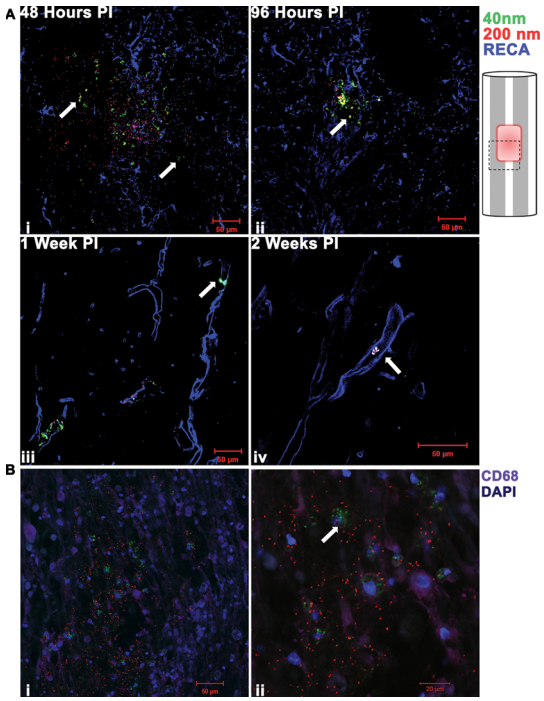

Figure 2. Nanoparticle extravasation is dependent on particle size and time post-SCI. (A) Micrographs of lesion epicenter as depicted in cartoon (dashed line) at (i) 48 h postinjury (PI); (ii) 96 h PI; (iii) 1 week PI; and (iv) 2 weeks PI. Particles with diameters of 40 nm (green) and 200 nm (red), but not 1000 nm (not shown), were able to extravasate into the spinal cord parenchyma for up to 96 h PI. Examples of particles in spinal cord tissue are indicated by white arrows. At 1 week and 2 weeks PI, particles were trapped in blood vessels (rat endothelial cell antigen staining, blue), as indicated by white arrows. (B) Nanoparticles are endocytosed by microglia/macrophages (i). Micrograph depicts that CD68+ (cyan) cells engulf extravasated nanoparticles, indicated by white arrow in (ii). Cell nuclei are stained with DAPI (blue). Dashed box represents zoomed-in region showed in (ii). Scale bars: (A,Bi) 50 μm; (Bii) 20 μm.

that some of the extravasated nanoparticles were phagocytosed by reactive microglia (CD68 staining) in the injured spinal cord (Figure 2Bi,ii). Taken together, these data indicate a 96 h time window of nanocarrier extravasation into the injured spinal cord for particles as large as 200 nm.

CSB Stealth Liposome Synthesis and Characterization. To deliver CSB *in vivo*, we synthesized liposomal nanoparticles encapsulating CSB (nano-CSB). We have previously delivered imaging agents[32,48,49] and chemotherapeutic drugs[31,50] using stealth liposomes that have PEG chains on their surface to enable their evasion of the reticuloendothelial system (RES). Using similar techniques, we developed stealth liposomes with a mean diameter of ~110 nm and a polydispersity index of 0.02, as assessed by dynamic light scattering (DLS, Figure 3A). Transmission electron microscopy confirmed the results obtained by DLS (Figure 3B). To ensure no free dye remained in solution, the liposomes were thoroughly washed and dialyzed. The liposomes stably encapsulated CSB in their aqueous phase at a concentration of 18 mg/mL. *In vitro*, the liposomes were engulfed by macrophages (Figure 3C), and blank liposome administration to cells in culture did not lead to inflammation over 48 h (Figure S2, Supporting Information).

***In Vivo* Effects of Liposomally Encapsulated CSB.** *Toxicity.* Adult male Sprague–Dawley rats were subjected to a clinically relevant contusion SCI at the T9 vertebral level using a force-controlled impaction device.[47] To evaluate the effects of CSB delivery in rats with SCI, we delivered liposomal CSB (nano-CSB, 25 mg/kg) intravenously, 48 h postinjury. Since there is no prior information available for the *in vivo* dosage of CSB in rats, we determined a maximum dosage of 40 mg/kg, based on a lowest toxic dose (TD_{lo}) value of 200 mg/kg in rats (as supplied by the manufacturer, Tocris Biosciences). The injury parameters of impact force and velocity were consistent across all groups (data not shown) and produced a well-defined injury over 96 h (Figure S3A,B, Supporting Information). Control animals received SCI but no interventions, and sham animals received a laminectomy but no injury. The nano-CSB was allowed to circulate for an additional 48 h, after which the animals were sacrificed for genomic analyses and immunofluorescence and histology. In order to determine if nano-CSB administration led to toxicity *in vivo*, we measured the level of TNF-α in the serum of control and drug-treated animals from blood collected at the time of sacrifice. The circulating levels of CSB in the serum of animals injected with nano-CSB (Figure S3C, Supporting Information) were ~2 μM. No differences were observed in the serum levels of TNF-α between nano-CSB-treated and control animals (Figure S3D, Supporting Information). The levels of TNF-α were close to the lower limits of detection, indicating no TNF-α elevation in the animals treated with our liposomal preparations and the CSB.

***In Vivo* Quantitative Gene Analysis.** To assess the changes in the expression of various inflammation related proteins, chemokines, and cytokines known to be regulated by MIF, we performed cytokine gene analysis on the spinal cords of the control and nano-CSB-treated animals using quantitative reverse transcription polymerase chain reaction (qRT-PCR). Five millimeter segments centered on the injury site were used for the genomic analysis.[51] Inflammation-associated transcripts were upregulated in the spinal cords of animals with SCI in comparison with sham-operated animals (Figure S4A, Supporting Information). Because MIF inhibition should modulate inflammation and wound healing, we assessed transcript levels of inflammatory mediators and those associated with resolution phase macrophages[52–56] (since macrophages and microglia are a major inflammation-associated cell type in SCI and nanoparticles are engulfed by these cells, Figure 2Bi,ii). Treatment with nano-CSB led to

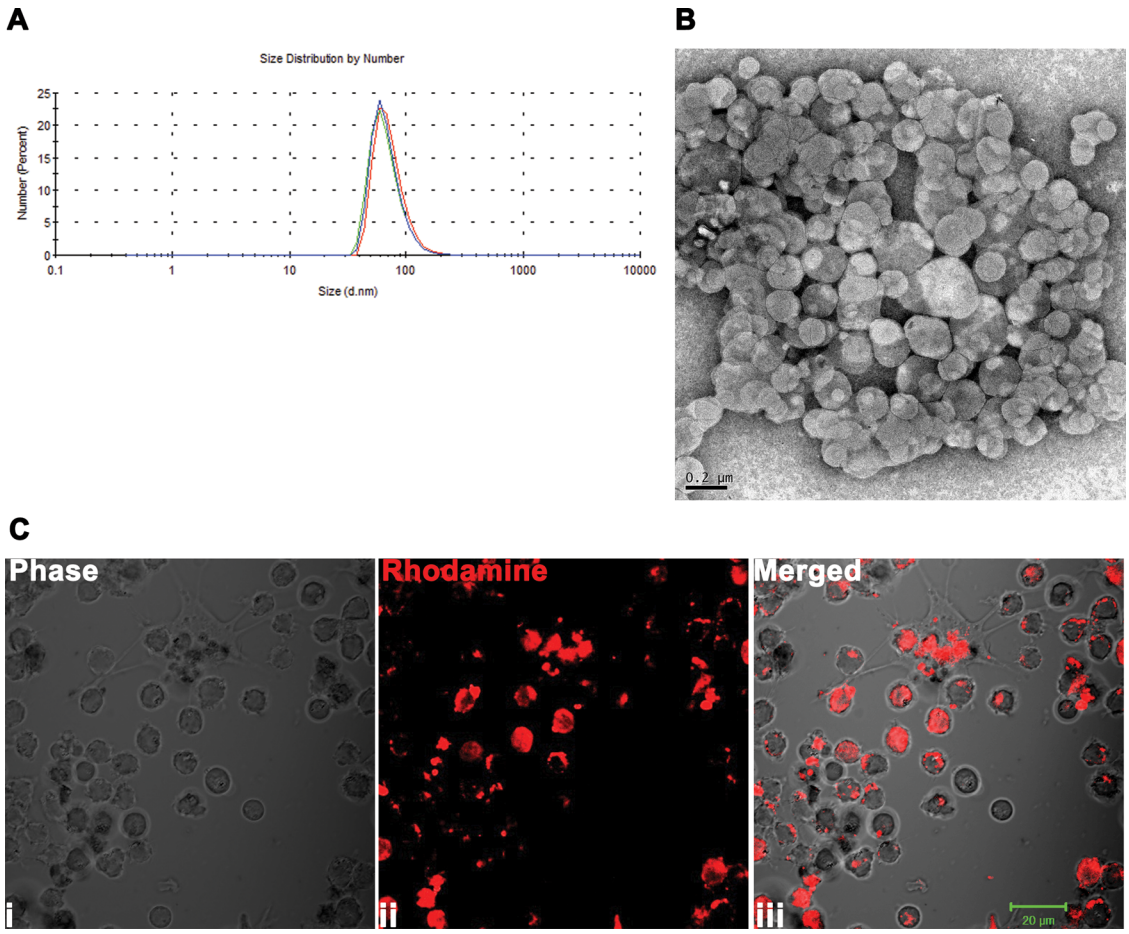

Figure 3. Size characterization and *in vitro* uptake of CSB liposomes. (A) Dynamic light scattering shows narrow size range of CSB liposomes with a mean diameter of 110 nm. (B) Transmission electron micrograph of CSB liposomes. Scale bar is 200 nm. (C) RAW 264.7 cells (i) engulf CSB liposomes (ii) labeled with rhodamine (red) and overlaid in (iii). Scale bar for (C) is 20 μm.

an increase in the expression of anti-inflammatory markers arginase I (Arg-I, $p < 0.05$) and tissue growth factor beta (TGF-β, $p < 0.1$, $p = 0.053$) and pro-inflammatory markers IL-1β ($p < 0.1$, $p = 0.052$), chemokine (C−C motif) ligand 2 (CCL2, $p < 0.05$), and induced nitric oxide synthase (iNOS, $p < 0.05$, Figure 4). *In vitro* cytokine analysis showed a similar profile in LPS-IFN-γ-activated macrophages treated with CSB (Figure S1B, Supporting Information). No differences were observed between groups for transcript levels of suppressors of cytokine signaling (SOCS) SOCS1, SOCS2, and SOCS3 (Figure S4B, Supporting Information). Furthermore, nano-CSB-treated animals showed a tendency for higher downregulation of MMP-1b transcripts, and the Toll-like receptors (TLR) TLR-2 ($p < 0.1$, $p = 0.052$) and TLR-4 ($p < 0.1$, $p = 0.066$) tended to show higher transcription in nano-CSB-treated animals (Figure S4C, Supporting Information). Finally, control animals showed a downregulation of NF-κB (nuclear factor-kappa B) transcripts, while nano-CSB treatment led to no change in NF-κB transcript levels in comparison with sham animals (Figure S4D, Supporting Information). Taken together, these data suggest that nano-CSB administration led to a hybrid inflammatory milieu comprising both pro- and anti-inflammatory transcripts.

***In Vivo* Immunohistochemistry.** Because MIF plays a critical role in wound healing,[57] and MIF knockout mice show improved neuronal survival and locomotor recovery after SCI,[18,20] we wanted to determine the effect of nano-CSB delivery on axonal integrity. To do this, we stained spinal cord tissue using luxol fast blue, a myelin-specific stain. Animals receiving nano-CSB had a higher amount of white matter sparing ($p < 0.05$) at the lesion site (Figure 5A,B) in comparison with the controls, while no differences were observed at other regions rostro-caudally. Significantly, animals receiving nano-CSB also showed an overall smaller rostro-caudal spread of injury in comparison with controls (Figure 5C,D). Next, we assessed blood vessel integrity and inflammation, as they are responsible for secondary degeneration following SCI[3,33] and resolution of vascular integrity leads to better functional outcomes. Blood vessel integrity was evaluated by staining for laminin.[33] Animals treated with nano-CSB showed better preservation of vascular integrity (Figure 6A−C) at the epicenter and at sites away from the injury ($p < 0.05$). To confirm the integrity of the vasculature, we assessed

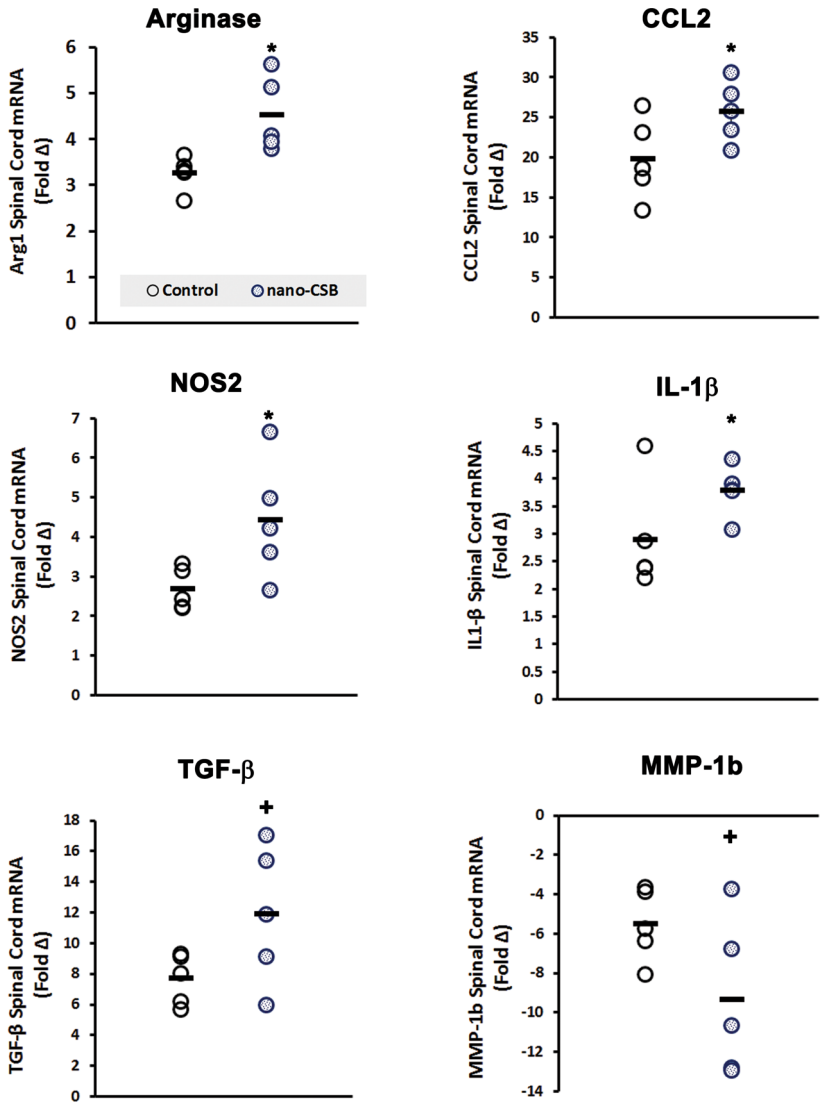

Figure 4. Nano-CSB alters the inflammatory milieu after SCI and leads to a hybrid inflammatory state. Five millimeter spinal segments centered on the injury site were excised for mRNA extraction. Data are normalized to internal housekeeping gene (HRPT-1) and expressed as fold change over sham animals that received laminectomy only. Quantitative RT-PCR reveals that nano-CSB treatment alters both pro- and anti-inflammatory mRNA levels at 96 h post-SCI. Nano-CSB treatment significantly increases pro-inflammatory markers CCL2, IL-1β, and iNOS levels while simultaneously increasing anti-inflammatory markers such as arginase I and TGF-β. Data are represented as mean (black bar) and individual data points. Means with *$p < 0.05$ are significantly different and means with $+p < 0.1$ tend to be different from controls.

the levels of extravasated plasma protein IgG[58,59] and found that animals treated with nano-CSB had significantly lower leakage of serum IgG into the spinal cord ($p < 0.05$, Figure 6D,E). Further, animals treated with nano-CSB tended to show higher levels of arginase staining ($p < 0.1$, $p = 0.07$), although no difference in total number of microglia/macrophages (as assessed by CD68 staining) was noted. Significantly, the ratio of arginase to $CD68^+$ cells was higher ($p < 0.05$) in nano-CSB-treated animals (Figure S5A–D, Supporting Information). Taken together, histological assessment of SCI animals showed that nano-CSB treatment led to improved tissue sparing, limited the spread of injury, improved the preservation of vascular integrity, and reduced IgG leakage.

DISCUSSION

Attenuation of secondary injury related inflammation is a critical treatment metric in SCI.[11] Therapeutic delivery systems that cause minimal trauma and enable site-specific drug delivery to reduce systemic side effects are important for achieving this goal in SCI treatment. While it has been reported that the BSB might be compromised for periods up to 4 weeks post-SCI, as assessed using small dyes or tracers,[58,60] permeability of the BSB to nanocarriers is not well-understood. Our results suggest that particles as large as 200 nm in diameter can extravasate into the injured spinal cord parenchyma up to 96 h post-SCI, but not beyond 1 week post-SCI. This indicates that using

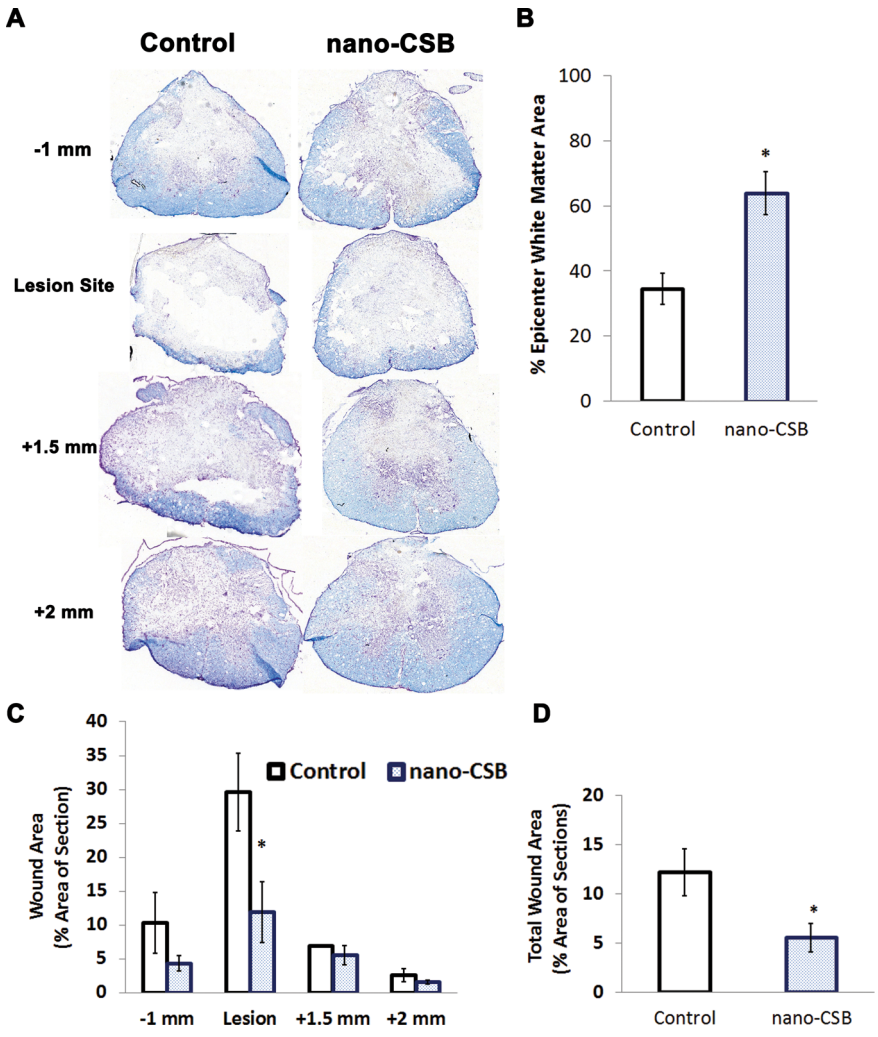

Figure 5. Nano-CSB leads to preservation of tissue and white matter integrity. (A) Spread of injury/tissue integrity visualized with luxol fast blue (for myelin) counterstained with cresyl violet staining on control and nano-CSB animals spanning distances 1 mm rostral and 2 mm caudal to the lesion site. (B) Nano-CSB treatment leads to significant white matter sparing. (C) Visually, wound margins are smaller for nano-CSB-treated animals at the lesion site but not at other locations. (D) Overall wound area is smaller in nano-CSB-treated animals. Data are represented as mean ± SEM. Means with *$p < 0.05$ are significantly different from control animals.

long-circulating nanocarriers such as liposomes can achieve site-specific drug delivery up to 96 h post-SCI through passive targeting.

Secondary injury is characterized by intense inflammation, and current clinical guidelines recommend the use of potent anti-inflammatory drugs which can lead to deleterious side effects.[12] Thus, there is a need to develop new, anti-inflammatory drug candidates. We chose a recently discovered MIF inhibitor, CSB, as an anti-inflammatory agent.[25] MIF is a pleiotropic cytokine that is an upstream mediator of pro-inflammatory processes. MIF secreted by macrophages is induced by glucocorticoids and counteracts the inhibitory effects of glucocorticoids on macrophage cytokine secretion, thereby maintaining a balance in immune function when glucocorticoid production is high, for example, in trauma.[57] This indicates that in situations where glucocorticoids are prescribed as therapeutics (inflammatory diseases such as multiple sclerosis, Alzheimer's disease, and SCI), MIF inhibition may play a pivotal role in potentiating the therapy.[16,17,57]

Koda *et al.*[18] demonstrated that MIF expression is upregulated after compression-induced SCI in rats, and Nishio *et al.* demonstrated that deletion of MIF attenuates neuronal death and promotes functional recovery after SCI in mice, while MIF exacerbated glutamate-induced cell death of cerebellar granular neurons.[20] Furthermore, Alexander *et al.*[61] reported that MIF null mice fail to develop pain-like behaviors in response to inflammatory stimuli or nerve injury. Recent reports have shown that serum levels of MIF are significantly higher even in humans with chronic SCI.[19] Thus, blocking the activity of MIF might be beneficial in SCI because it could confer neuroprotection, aid in functional recovery, provide analgesia, and potentiate the action of glucocorticoids (both endogenously produced and externally administered).

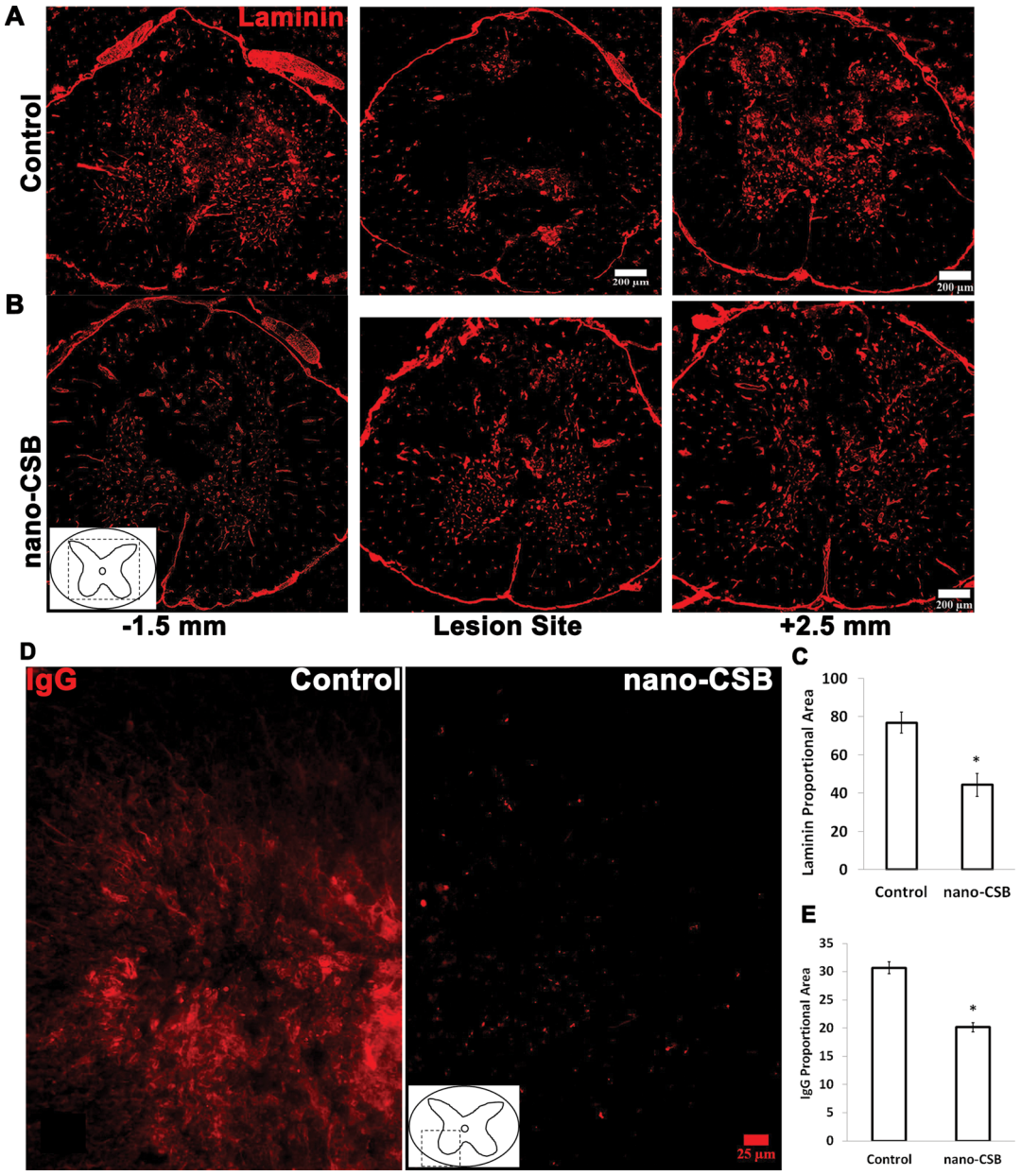

Figure 6. Nano-CSB treatment leads to the preservation of blood vessels and decreases IgG extravasation. Blood vessel integrity is identified by laminin-positive (red) basement membrane in the injury penumbra and the caudal and rostral regions of control (A) and nano-CSB-treated (B) animals. Note that blood vessels look normal in nano-CSB-treated animals, and the large deposits of laminin in control animals indicate tissue loss and scarring at sites away from the lesion site. (C) Total laminin-positive area showed a significant reduction after nano-CSB treatment compared to controls. (D) Representative IgG staining in the ventral horn and surrounding white matter at the lesion site, showing significantly reduced IgG leakage in nano-CSB-treated animals and quantified in (E). The dashed box in the inset shows regions where the data were quantified from. Data are mean ± SEM, and means with *$p < 0.05$ are significantly different.

We investigated CSB's effectiveness in targeting inflammation after SCI because CSB is a potent inhibitor of MIF tautomerase activity.[25] Additionally, CSB is a vesicular glutamate transporter inhibitor preventing uptake of glutamate by neurons[26−28] and has been shown to exert anti-nociceptive effects without affecting spontaneous locomotor activity of mice.[26] Thus, CSB can potentially target and alleviate MIF-mediated inflammation, glutamate-mediated excitotoxicity, and provide analgesia after SCI, although we did not evaluate the latter two aspects in this study. Furthermore, CSB is highly water-soluble, making it an ideal candidate for drug delivery and liposomal encapsulation. Consistent with the results of Bai *et al.*[25] and others[23] who have studied the effects of MIF inhibition *in vitro*, we observed that CSB demonstrated anti-inflammatory effects on a variety of macrophage cell types including primary macrophages and microglia, while exhibiting little cytotoxicity even at high doses *in vitro*.

In vivo administration of nano-CSB in rats with SCI led to preservation of tissue and blood vessel integrity. MIF plays a critical role in diseases such as stroke, cancer, rheumatoid arthritis, sepsis, colitis, and multiple sclerosis (MS).[17,24,62] In the context of MS, MIF inhibition reduced the severity of the disease, improved remyelination, and prevented entry of immune cells in the brain and spinal cord of mice by modulating blood−brain barrier function in a mouse model of MS.[63,64] Because inflammatory cytokines and MMPs lead to BSB disruption[65,66] and MIF inhibition is anti-inflammatory and blocks MMP activity,[17] MIF inhibition can lead to restoring BSB integrity, as can targeted anti-inflammatory therapy.[67] Accordingly, our *in vivo* results also showed improved white matter integrity and reduced BSB leakage in nano-CSB-treated animals.

However, quantitative gene analysis showed that animals receiving nano-CSB exhibited a hybrid inflammatory milieu. Transcript levels of arginase I, iNOS, IL-1β, and CCL2 were significantly higher in comparison with control animals with SCI, while MMP-1b levels tended to be lower. While it is known that arginase I is a marker for alternatively activated macrophages, which are anti-inflammatory in nature, iNOS, IL-1β, and CCL2 (which were downregulated by CSB *in vitro*) are typically considered to be inflammatory.[53,56,68,69] We postulate that the unexpected promiscuity in inflammatory transcript expression *in vivo* is likely due to the timing of nano-CSB administration. CSB was administered 48 h postinjury, when inflammation was already established. One reason to intervene late after SCI onset in this study was to take advantage of the homeostasis-promoting effect of inflammation, wherein early suppression of inflammation has been shown to have negative effects on wound healing after SCI.[70,71] Recent work[53,66,68] has shown that an intact inflammatory response by microglia may be protective in the context of SCI.

Additionally, CSB could have differential potential toward downregulating MIF activity, which means that, while CSB actively prevents the inflammatory activity of MIF, it may only partially block the chemokine activity of MIF.[25] Indeed, our *in vitro* results show that, while CSB can potently suppress secretion of inflammatory mediators like TNF-α, IL-6, and nitrite, it only partially suppresses chemokines like CCL2 and macrophage inhibitory protein (MIP)-1α and MIP-1β (Supporting Information Figure S1) responsible for recruitment of monocytes and other myeloid cells, which could lead to incomplete suppression of inflammation but may also lead to homeostasis.[71,72] Since the SCI environment is quite complex with multiple activated inflammatory pathways, inflammation may only be partially suppressed by MIF inhibition. Therefore, CSB-mediated MIF inhibition remains a potentially attractive approach as discussed below.

Regarding the promiscuous triggering of both anti- and pro-inflammatory signals after CSB administration, it has been shown that macrophages respond dynamically to their microenvironment and can exhibit hybrid phenotypical states (termed as M2C/M2D macrophages[56,73]), wherein they express both pro- and anti-inflammatory markers and are reparative in nature.[53,74] Indeed, Fenn *et al.*[53] showed that adult mice that exhibited better wound repair after SCI in comparison with aged mice had enhanced IL-1β and CCL2 mRNA expression. Similarly, Stirling *et al.*[68] demonstrated that a mixed microglial activation state (expressing both pro- and anti-inflammatory markers) is beneficial and prevents secondary injury induced demyelination of white matter tracts. Significantly, Stirling *et al.*[68] showed that treatments aimed at suppressing macrophage activation (by inhibition of CCL2, IL-1β, and iNOS) were ineffective and exacerbated tissue damage in SCI.[75] Both Fenn *et al.*[53] and Stirling *et al.*[68] demonstrated restriction of tissue pathology in a microenvironment that favored a hybrid inflammatory state, and this result was also observed by us. In support of this wound resolution state,[76] we also observed that TGF-β transcript levels tended to be elevated in nano-CSB-treated rats. The pleiotropic cytokine TGF-β positively regulates arginase activity in macrophages,[77] is important for the constitution of a normal vascular network in the healing wound,[78] and is expressed by the wound-healing M2C phenotype of macrophages,[52,55,56,79] and exogenous administration of TGF-β has been shown to reduce the lesion size in SCI animals.[80] Since we did not specifically isolate mRNA from microglia in the injured spinal cord, we cannot ascribe our results solely to microglia or macrophages, and we expect that other glial cells are involved.[67] However, since nanoparticles are engulfed by phagocytic cells such as macrophages, microglia, and neutrophils, it is reasonable to expect that the effects observed are in part also mediated by these cells. Animals treated with nano-CSB also showed a tendency for higher transcription of TLR2 and 4. Signaling *via* the TLRs is important for regulating the pathophysiology of SCI and TLR2, and TLR4-deficient mice show excessive myelin loss.[66] Furthermore, control animals showed a downregulation of NFκB (nuclear factor kappa-B) transcripts, while nano-CSB treatment led to no change in NFκB transcript levels in comparison with sham animals. The precise roles of NFκB signaling in traumatic CNS injury are complicated and unresolved.[81−83] However, NFκB downregulation has been shown to lead to increased MIF levels and oxidative stress.[84] Thus, return of NFκB transcript levels to a basal state may be beneficial. Taken together, nano-CSB administration led to an overall hybrid pro-resolution inflammatory state which may be beneficial in treating SCI.

While the results from this acute study are promising, the long-term effects of CSB administration and dosing on functional recovery post-SCI and toxicity need further evaluation. We observed low levels of CSB in the serum of animals even after 48 h postinjection. Sustained presence of glutamate uptake blockers such as CSB may cause neurotoxicity chronically,[85] thereby making a case against the use of free CSB. The use of liposomal forms of CSB will certainly alleviate systemic toxicity associated with free drugs while providing site-specific delivery. Stealth liposomes coated by PEG have improved circulation time because the PEG stabilizes and protects the liposomes from opsonization and are cleared by the liver and spleen or blood macrophages over time.[35,86,87] Liposomes, by virtue of being biocompatible, biodegradable, nontoxic, having long circulation times, and being approved by the FDA, are ideal drug delivery vehicles for sites of trauma such as the brain and spinal cord, where implantable devices can cause irreversible damage.

CONCLUSIONS

In this study, we have demonstrated that the BSB is permeable to nanoparticles as large as 200 nm for up to 96 h post-SCI, providing a long time window for therapeutic administration using nanoparticles. Using long circulating liposomes as drug nanocarriers that fit this size profile, we demonstrated the beneficial effects of a novel small molecule inhibitor of MIF (CSB) in a clinically relevant rat model of SCI. Liposomal CSB improved BSB integrity, protected axons from demyelination, and modulated the inflammatory milieu to a hybrid pro-resolution reparative state.

EXPERIMENTAL SECTION

Animal Model of Spinal Cord Injury. All procedures were approved by the Institutional Animal Care and Use Committee at the Georgia Institute of Technology. Adult male Sprague–Dawley rats (2–4 months old, 300–350 g, Charles River) were used for all studies (n = 4–6 animals per experimental group). Surgeries were performed in sterile conditions as described before.[88] Briefly, rats were deeply anesthetized using isoflurane and received a laminectomy at vertebral level T9 (sham experimental group) or a laminectomy followed by a moderate spinal cord contusion using the force control mode on an Infinite Horizons device (150 kdyne; Precision Systems and Instrumentation).[89] Rats were allowed to recover under a warming lamp and administered 3 mL of sterile saline and slow release buprenorphine intramuscularly. Rats were then single housed until further interventions and had access to food and water *ad libitum*. Rats receiving a spinal cord contusion underwent bladder expression twice daily for the duration of the experiment.

Nanoparticle Extravasation Study. Latex nanoparticles coated with carboxylic acid terminal groups for long circulation times were purchased from Invitrogen (Fluospheres, 2–5% solids). The particles were 40 nm (ex/em: 505/515 nm), 200 nm (ex/em: 580/605 nm), and 1000 nm (ex/em: 350/440 nm) in size to span 3 orders of magnitude of diameter and had distinct fluorescent spectra. Beads were administered according to methods described by Sawyer *et al.*[41] Briefly, at 48 h, 96 h, 1 week, or 2 weeks postinjury, animals were intravenously (*via* the tail vein) administered a 200 μL solution cocktail with three different sized (40, 200, and 1000 nm) nanoparticles each at 0.5%, brought up to 1 mL in sterile saline. Animals were transcardially perfused and fixed with 500 mL each of PBS and 4% paraformaldehyde (PFA) 6 h after the injection of nanoparticles. Spinal cords were dissected out and postfixed overnight in 4% PFA in PBS and subsequently in 30% sucrose solution in PBS for 48 h for cryoprotection, after which spinal cords were frozen and prepared for cryosectioning.

Preparation and Characterization of CSB-Encapsulating Liposomes. 1,2-Dipalmitoyl-*sn*-glycero-3-phosphocholine (DPPC, Genzyme), cholesterol (Sigma-Aldrich), and 1,2-distearoyl-*sn*-glycero-3-phosphoethanolamine-*N*-[methoxy(poly(ethylene glycol))-2000] ($mPEG_{2000}$-DSPE, Genzyme) were used for preparing the liposomes.[32,49] Dialysis tubing with a 3500 Da molecular weight cutoff (MWCO) was obtained from Spectra/Por (Dominguez, CA, USA). Chicago sky blue was purchased from Tocris Biosciences. Liposomes containing CSB were prepared according methods described previously.[32,49] Briefly, DPPC, cholesterol, and DSPE-PEG were dissolved in ethanol in a molar ratio of 65:30:5, respectively. In some cases, to fluorescently label the liposomes, 1,2-dipalmitoyl-*sn*-glycero-3-phosphoethanolamine-*N*-(lissamine rhodamine B sulfonyl) (Liss rhodamine PE, Avanti Polar Lipids) was added at a molar ratio of 0.1. After the lipids were dissolved in ethanol at 65 °C, CSB (72 mg/mL) dissolved in PBS was added to the lipids. The ratio of ethanol to PBS was 1:10 by volume. The lipid–CSB solution was gently stirred at 65 °C for 1 h to allow for hydration. At the end of 1 h, the liposome–CSB solution was washed five times with excess PBS by centrifugation at 20 000g for 20 min to remove excess free dye at 4 °C. Subsequently, liposomes were resuspended in the original volume of PBS and sonicated for 1 h at 65 °C. After sonication, liposomes were sequentially extruded at high pressure at 65 °C on a Lipex Thermoline extruder (Northern Lipids, Vancouver, Canada) with three passes through a 1.0 μm nucleopore membrane, three passes through 0.8 μm nucleopore membrane, five passes through a 0.4 μm nucleopore membrane, five passes through a 0.2 μm nucleopore membrane, and 10 passes through a 0.1 μm nucleopore membrane, followed by exhaustive dialysis against sterile PBS solution in a 3500 Da MWCO dialysis membrane to remove any remaining free CSB. This method of liposome preparation was adopted to ensure that there would be no leakage of CSB, which was completely encapsulated in the stealth liposomes.[32,49] Blank liposomes were made similarly by hydrating the lipid mixture with PBS. The stealth nature of liposomes bestows a long circulatory nature to this contrast agent since the PEG in the liposomal system prevents uptake by the RES system. The particle size of the liposomes was determined by dynamic light scattering at 25 °C (Zetasizer, Malvern Instruments). For morphological characterization of the liposomes, the liposomes were frozen at −80 °C, lyophilized overnight using a Labconco freeze-drier system, and prepared for transmission electron microscopy (TEM) on a Zeiss-Ultra 60 field emission TEM. To determine the amount of CSB encapsulated within the liposomes, liposomes were lysed by dissolving the lipid phase in ethanol and extracting the aqueous phase containing CSB by centrifugation. The aqueous phase was then lyophilized, and the amount of encapsulated CSB (adjusted for weight of salts in PBS) was estimated.

Drug Delivery Post-SCI. At 48 h postinjury, liposomal CSB (nano-CSB, 25 mg/kg) was delivered intravenously *via* the tail vein as described above. At 48 h postinjection (96 h postinjury), animals were transcardially perfused and spinal cord sections saved for genomic analysis and immunohistochemical and immunofluorescent staining.

qRT-PCR Analysis of Spinal Cords Following Injury. *Spinal Cord Segment Collection.* Spinal cord segments were collected 96 h postinjury according to methods described by Butt *et al.*[51]

To minimize degradation of spinal cord samples, anesthetized rats were transcardially perfused with 1000 mL of ice-cold sterile PBS. The rats were then placed on a metal block cooled by ice, and a laminectomy of the entire thoracic and lumbar spinal cord was performed. The isolated spinal cord was kept on ice while a 5 mm segment centered on the injury site was excised. The excised segments were placed in precooled (4 °C) sterile RNase/DNase-free microcentrifuge tubes and immediately flash frozen in liquid nitrogen. All cord segments were stored at −80 °C until further processing.

Ribonucleic Acid (RNA) and Protein Extraction. RNA was extracted from the spinal cord segments according to methods described by Butt *et al.*[51] with minor modifications. Briefly, RiboZol RNA extraction reagent mediated extraction of total RNA, and subsequent extraction of protein was carried out essentially according to the manufacturer's specifications (Amresco) with minor modifications. To a 5.0 mm spinal cord segment was added 0.5 mL of RiboZol, and the sample was homogenized with an RNase-free pestle for 30 s manually, after which 0.5 mL more of RiboZol was added. The sample was further homogenized by passing through a 20 gauge needle and syringe. Following incubation for 5−10 min at room temperature, 0.2 mL of chloroform/mL of RiboZol was added, and the tubes were shaken vigorously for 15 s and then incubated for 2−3 min at room temperature. This mixture was then centrifuged at 12 000*g* for 15 min at 4 °C. The aqueous phase was transferred to a new tube; an equal volume of 200 proof anhydrous ethanol was added, and the solutions were mixed and immediately transferred to an RNeasy spin column (RNeasy Plus Mini Kit, QIAGEN); RNA was extracted according to the kit's instructions along with an on-column DNase treatment. RNA was eluted in water and stored at −80 °C until further analysis.

Quantitative Real-Time Polymerase Chain Reaction (qRT-PCR) Analysis. RNA concentration and quality was determined using a UV spectrophotometer (Nanodrop, Thermo Scientific, Waltham, MA) and denaturing agarose RNA gel electrophoresis. qRT-PCR primers for the genes listed in Table S1 (Supporting Information) were purchased from SA Biosciences. cDNA was prepared using the RT^2 first strand cDNA synthesis kit (QIAGEN, CA) according to the manufacturer's directions. qRT-PCR was carried out using the Fluidigm BioMark Genetic Analysis Platform utilizing Dynamic Array Integrated Fluidic Chip technology. Each sample was run in triplicate, and expression of the genes listed in Table S1 (Supporting Information) was calculated (n = 5−6 animals/condition). Data were normalized to the reference gene (HRPT-1) and expressed as fold change over sham animals that received laminectomy only, using the $\Delta\Delta Ct$ calculation method.[90]

Immunohistochemistry and Immunofluorescence. Immunohistochemistry and immunofluorescent staining was performed according to methods described previously.[88] Briefly, animals were anesthetized using ketamine (50 mg/kg)/xylazine (10 mg/kg)/acepromazine (1.67 mg/kg) and transcardially perfused with 0.1 M PBS followed by 4% PFA. Following laminectomy, a 10 mm segment centered on the injury epicenter was cut, and the tissue was cryoprotected with 30% sucrose for 48 h following postfixation. Spinal cord segments were rapidly frozen in OCT compound. Serial transverse/coronal or longitudinal sections (18 μm thick) were cut using a Microm HM550 cryostat (Mikron Instruments) and collected on glass slides. For immunofluorescent staining, sections were stained with antibodies listed in Table S2 (Supporting Information). Briefly, serial sections were blocked with blocking buffer (PBS containing 10% BSA, 4% goat serum, and 0.5% Triton-X100) for 1 h and incubated overnight in blocking buffer containing groups of antibodies (Table S2, Supporting Information). Following primary antibody incubation, the sections were washed three times with PBS and blocked for 1 h in PBS containing 1:220 dilutions of appropriate secondary antibodies (Table S2, Supporting Information). After 1 h, sections were washed several times with PBS and stained for 15 min with 4′,6-diamidino-2-phenylindole (DAPI) nuclear stain (Life Technologies, NY). Tissue sections were subsequently washed three times with PBS and coverslipped with Fluormount-G (Southern Biotech, AL). Sections were stored at 4 °C until imaged. For histological staining, samples were stained with hematoxylin and eosin to assess gross tissue structure and integrity, and with luxol fast blue (LFB) counterstained with cresyl violet (CV) for assessing white matter sparing. To measure epicenter tissue sparing, images were taken at the epicenter and up to 200 μm rostral and caudal of the epicenter. For all tissues, three representative images from each sample were taken for analysis. Fluorescent images were taken with a Zeiss 710 NLO confocal microscope, or tissue sections were imaged on a Zeiss Axiovert 200 M (Carl Zeiss, NY) using equal exposure times for all fluorescent markers across all groups. Hematoxylin and eosin, LFB, and CV images were taken with a Carl Zeiss Axioplan 2 Imaging microscope. Quantification of fluorescent and phase images was done using ImageJ NIH software[91] according to previously published methods.[33,53] For fluorescent image quantification (laminin, IgG, CD68, and arginase), images from four locations (1.5 or 2 mm rostral to lesion site, at the lesion site, 1.5 or 2 mm caudal to lesion site, and 2 or 2.5 mm caudal to lesion site; please see figure legends for appropriate distances) for each animal (n = 3 animals/condition) were imported into ImageJ, and a region of interest (ROI, consistent across all images) was selected. ROIs for CD68, arginase, and laminin ecompassed the dorsal and ventral horns of the gray matter and the adjacent white matter, whereas the ROI for IgG encompassed only the ventral horn and the ventral funiculus. The ROI was analyzed using the plot profile tool in ImageJ, which creates a "column average plot", where the x-axis represents the horizontal distance through the selection and the y-axis represents the vertically averaged pixel intensity. The averaged pixel intensities were imported into spreadsheet software (Microsoft Excel), and an integrated intensity value at each rostrocaudal distance was obtained by summing the ordinate values. These values were averaged across an animal to provide a final average intensity value per animal. In cases where only the lesion site was analyzed, three images per animal at the lesion site were taken and subjected to the same procedure. Average intensity values were statistically analyzed.

***In Vitro* Cell Culture Studies.** *Primary Cell Culture.* Primary astrocytes and microglia were obtained according to methods previously published.[92] Briefly, postnatal day 1 (P1) Sprague−Dawley pups were anesthetized using 4% isoflurane and quickly decapitated. The brains were removed and freed of the associated meninges. The cerebral cortices were carefully dissected, rinsed three times in ice-cold Hank's balanced salt solution (HBSS) (Mediatech, Inc., VA) and minced in a Petri dish. The minced tissue obtained from 3 to 5 pups was trypsinized using 3.5 mL of 0.25% trypsin EDTA (Mediatech, Inc., VA) at 37 °C for 10 min, following which trypsin was inactivated by the addition of ice-cold DMEM F12 50/50 (Mediatech, Inc., VA) with 10% FBS (Gemini Bio-Products, CA). The trypsinized tissue was washed three times with ice-cold HBSS and finally resuspended in 3.5 mL of HBSS. Then 300−500 μL of DNase (1.5 mg/mL) (Sigma-Aldrich, MO) was added and triturated gently until the tissue clumps disappeared. The cell suspension was centrifuged at 1000*g* for 3 min, and the supernatant was discarded. The cell pellet was resuspended in plating media (DMEM F12 50/50 containing 10% FBS and 1% penicillin/streptomycin) and plated in a T-75 flask. Twenty-four hours after plating, the flask was shaken to dislodge microglia, which were plated in a separate T-75 flask. The first flask was rinsed with prewarmed HBSS and replenished with plating media. The process was repeated again on day 2, resulting in >95% pure astrocytes which gained confluence in approximately 1 week. Microglial cultures were isolated 10−14 days after shaking the second flask for 1 h at 37 °C. Mixed glial cultures containing astrocytes and microglia were also maintained. Furthermore, pure astrocyte cultures from e18 rats were also purchased from BrainBits LLC and cultured according to provided instructions.

Primary bone marrow derived macrophages were obtained according to methods described previously[93] Briefly, 6−10 week old BALB/c mice (The Jackson Laboratory) were sacrificed by CO_2 asphyxiation, and the abdomen and hind legs were sterilized with 70% ethanol. The femurs and tibias were collected, and muscle tissue was removed from the bones. Ends of the bones were cut, and the bone marrow was flushed into sterile Petri dishes with cell culture media using a syringe and a

25-gauge needle. The cells were suspended by pipetting up and down and passing the cells through a 70 μm cell strainer. Red blood cells were lysed with red blood cell lysis buffer (Sigma), washed two times with 2% fetal bovine serum (FBS) (Atlanta Biologicals) in phosphate buffered saline, and cultured in RPMI 1640 (HyClone) supplemented with 10% FBS, penicillin/streptomycin (100 U/mL), and recombinant murine M-CSF (20 ng/mL; Peprotech). Every 2 days, half of the cell media was replaced with fresh media. Experiments were performed on the adherent cells after 8 days of culture.

Cell Lines. The RAW 264.7 macrophage cell line from mouse was purchased from ATCC and cultured according to supplied instructions in DMEM supplemented with 10% FBS, 100 U/mL penicillin/streptomycin, and 1% L-glutamine.

Cell Activation. Primary cells and cell lines were activated with lipopolysaccharide according to methods described previously.[15,43] Briefly, cells were plated at 150 000−200 000 cells/well of a 12-well plate in respective complete media and allowed to attach overnight. The next day, cells were pretreated with recombinant mouse or rat IFN-γ (100 U/mL, R and D Systems) in low serum containing DMEM (0.5% serum for macrophages, and 2% serum for glial cells) for 1 h at 37 °C, following which LPS was added at 10 ng/mL. Cells were activated for 24 h, after which the medium was aspirated out and replaced with fresh low serum media with or without CSB (10 μM). Cells were incubated with CSB containing media for 24 h following which cells and conditioned media were collected for qRT-PCR and cytokine assays.

Statistical Analysis. A F-test was run to determine if the variances between the two groups being tested was equal, and based on the outcome, the appropriate Student's *t* test was used to assess significance between the means of nano-CSB-treated and control animals. Values were considered significant at $p < 0.05$ and a tendency at $p < 0.1$.[53]

Conflict of Interest: The authors declare no competing financial interest.

Acknowledgment. This study was funded by generous support from Tom Claugus, the Georgia Research Alliance and the Wallace H. Coulter Foundation, and a seed grant from the Children's Healthcare of Atlanta Center for Pediatric Nanomedicine at Georgia Institute of Technology and Emory University.

Supporting Information Available: In vitro activity of CSB, *in vivo* concentration and toxicity of CSB, *in vivo* transcript regulation of inflammation related genes, and immunohistochemical staining of spinal cords. This material is available free of charge *via* the Internet at http://pubs.acs.org.

REFERENCES AND NOTES

1. Silver, J.; Miller, J. H. Regeneration beyond the Glial Scar. *Nat. Rev. Neurosci.* **2004**, *5*, 146–156.
2. Fawcett, J. W.; Asher, R. A. The Glial Scar and Central Nervous System Repair. *Brain Res. Bull.* **1999**, *49*, 377–391.
3. Tator, C. H.; Fehlings, M. G. Review of the Secondary Injury Theory of Acute Spinal-Cord Trauma with Emphasis on Vascular Mechanisms. *J. Neurosurg.* **1991**, *75*, 15–26.
4. Hagg, T.; Oudega, M. Degenerative and Spontaneous Regenerative Processes after Spinal Cord Injury. *J. Neurotrauma* **2006**, *23*, 264–280.
5. Hall, E. D. Antioxidant Therapies for Acute Spinal Cord Injury. *Neurotherapeutics* **2011**, *8*, 152–167.
6. Donnelly, D. J.; Popovich, P. G. Inflammation and Its Role in Neuroprotection, Axonal Regeneration and Functional Recovery after Spinal Cord Injury. *Exp. Neurol.* **2008**, *209*, 378–388.
7. Popovich, P. G.; Whitacre, C. C.; Stokes, B. T. Inflammation, Autoimmunity and Spinal Cord Injury. *Shock* **1999**, *12*, 2–2.
8. Kigerl, K. A.; Gensel, J. C.; Ankeny, D. P.; Alexander, J. K.; Donnelly, D. J.; Popovich, P. G. Identification of Two Distinct Macrophage Subsets with Divergent Effects Causing Either Neurotoxicity or Regeneration in the Injured Mouse Spinal Cord. *J. Neurosci.* **2009**, *29*, 13435–13444.
9. Hausmann, O. Post-traumatic Inflammation in Spinal Cord Injury. *Spinal Cord* **2003**, *41*, 369–378.
10. Popovich, P. G.; Wei, P.; Stokes, B. T. Cellular Inflammatory Response after Spinal Cord Injury in Sprague−Dawley and Lewis Rats. *J. Comp. Neurol.* **1997**, *377*, 443–464.
11. Wing, P.; Dalsey, W.; Alvarez, E. Early Acute Management in Adults with Spinal Cord Injury: A Clinical Practice Guideline for Health-Care Professionals. *J. Spinal Cord Med.* **2008**, *31*, 408–479.
12. Breslin, K.; Agrawal, D. The Use of Methylprednisolone in Acute Spinal Cord Injury: A Review of the Evidence, Controversies, and Recommendations. *Pediatr. Emerg. Care* **2012**, *28*, 1238–1248.
13. Bracken, M. B.; Shepard, M. J.; Holford, T. R.; Leo-Summers, L.; Aldrich, E. F.; Fazl, M.; Fehlings, M.; Herr, D. L.; Hitchon, P. W.; Marshall, L. F.; et al. Administration of Methylprednisolone for 24 or 48 h or Tirilazad Mesylate for 48 h in the Treatment of Acute Spinal Cord Injury: Results of the Third National Acute Spinal Cord Injury Randomized Controlled Trial. *JAMA* **1997**, *277*, 1597–1604.
14. Fehlings, M. G.; Perrin, R. G. The Timing of Surgical Intervention in the Treatment of Spinal Cord Injury: A Systematic Review of Recent Clinical Evidence. *Spine* **2006**, *31*, S28–S35.
15. Calandra, T.; Bernhagen, J.; Mitchell, R. A.; Bucala, R. Macrophage Is an Important and Previously Unrecognized Source of Macrophage-Migration Inhibitory Factor. *J. Exp. Med.* **1994**, *179*, 1895–1902.
16. Calandra, T.; Bucala, R. Macrophage Migration Inhibitory Factor (MIF): A Glucocorticoid Counter-regulator within the Immune System. *Crit. Rev. Immunol.* **1997**, *17*, 77–88.
17. Calandra, T.; Roger, T. Macrophage Migration Inhibitory Factor: A Regulator of Innate Immunity. *Nat. Rev. Immunol.* **2003**, *3*, 791–800.
18. Koda, M.; Nishio, Y.; Hashimoto, M.; Kamada, T.; Koshizuka, S.; Yoshinaga, K.; Onodera, S.; Nishihira, J.; Moriya, H.; Yamazaki, M. Up-regulation of Macrophage Migration-Inhibitory Factor Expression after Compression-Induced Spinal Cord Injury in Rats. *Acta Neuropathol.* **2004**, *108*, 31–36.
19. Stein, A.; Panjwani, A.; Sison, C.; Rosen, L.; Chugh, R.; Metz, C.; Bank, M.; Bloom, O. Pilot Study: Elevated Circulating Levels of the Proinflammatory Cytokine Macrophage Migration Inhibitory Factor in Patients with Chronic Spinal Cord Injury. *Arch. Phys. Med. Rehabil.* **2013**, *94*, 1498–1507.
20. Nishio, Y.; Koda, M.; Hashimoto, M.; Kamada, T.; Koshizuka, S.; Yoshinaga, K.; Onodera, S.; Nishihira, J.; Okawa, A.; Yamazaki, M. Deletion of Macrophage Migration Inhibitory Factor Attenuates Neuronal Death and Promotes Functional Recovery after Compression-Induced Spinal Cord Injury in Mice. *Acta Neuropathol.* **2009**, *117*, 321–328.
21. Emmetsberger, J.; Tsirka, S. E. Microglial Inhibitory Factor (MIF/TKP) Mitigates Secondary Damage Following Spinal Cord Injury. *Neurobiol. Dis.* **2012**, *47*, 295–309.
22. Gensel, J. C.; Donnelly, D. J.; Popovich, P. G. Spinal Cord Injury Therapies in Humans: An Overview of Current Clinical Trials and Their Potential Effects on Intrinsic CNS Macrophages. *Expert Opin. Ther. Targets* **2011**, *15*, 505–518.
23. Al-Abed, Y.; Dabideen, D.; Aljabari, B.; Valster, A.; Messmer, D.; Ochani, M.; Tanovic, M.; Ochani, K.; Bacher, M.; Nicoletti, F.; et al. ISO-1 Binding to the Tautomerase Active Site of MIF Inhibits Its Pro-inflammatory Activity and Increases Survival in Severe Sepsis. *J. Biol. Chem.* **2005**, *280*, 36541–36544.
24. Morand, E. F.; Leech, M.; Jurgen, B. MIF: A new Cytokine Link Between Rheumatoid Arthritis and Atherosclerosis. *Nat. Rev. Drug Discovery* **2006**, *5*, 399–410.
25. Bai, F.; Asojo, O. A.; Cirillo, P.; Ciustea, M.; Ledizet, M.; Aristoff, P. A.; Leng, L.; Koski, R. A.; Powell, T. J.; Bucala, R.; Anthony, K. G. A Novel Allosteric Inhibitor of Macrophage Migration Inhibitory Factor (MIF). *J. Biol. Chem.* **2012**, *287*, 30653–30663.
26. Yu, G.; Yi, S.; Wang, M.; Yan, H.; Yan, L.; Su, R.; Gong, Z. The Antinociceptive Effects of Intracerebroventricular Administration of Chicago Sky Blue 6B, a Vesicular Glutamate Transporter Inhibitor. *Behav. Pharmacol.* **2013**, *24*, 653–658.

27. Roseth, S.; Fykse, E. M.; Fonnum, F. Uptake of L-Glutamate into Rat-Brain Synaptic Vesicles: Effect of Inhibitors That Bind Specifically to the Glutamate Transporter. *J. Neurochem.* **1995**, *65*, 96–103.
28. He, Z.; Yan, L.; Yong, Z.; Dong, Z.; Dong, H.; Gong, Z. Chicago Sky Blue 6B, a Vesicular Glutamate Transporters Inhibitor, Attenuates Methamphetamine-Induced Hyperactivity and Behavioral Sensitization in Mice. *Behav. Brain. Res.* **2013**, *239*, 172–176.
29. Mitragotri, S.; Burke, P. A.; Langer, R. Overcoming the Challenges in Administering Biopharmaceuticals: Formulation and Delivery Strategies. *Nat. Rev. Drug Discovery* **2014**, *13*, 655–672.
30. Tyler, J. Y.; Xu, X. M.; Cheng, J. X. Nanomedicine for Treating Spinal Cord Injury. *Nanoscale* **2013**, *5*, 8821–8836.
31. McNeeley, K. M.; Karathanasis, E.; Annapragada, A. V.; Bellamkonda, R. V. Masking and Triggered Unmasking of Targeting Ligands on Nanocarriers To Improve Drug Delivery to Brain Tumors. *Biomaterials* **2009**, *30*, 3986–3995.
32. Ayyagari, A. L.; Zhang, X.; Ghaghada, K. B.; Annapragada, A.; Hu, X.; Bellamkonda, R. V. Long-Circulating Liposomal Contrast Agents for Magnetic Resonance Imaging. *Magn. Reson. Med.* **2006**, *55*, 1023–1029.
33. Han, S.; Arnold, S. A.; Sithu, S. D.; Mahoney, E. T.; Geralds, J. T.; Tran, P.; Benton, R. L.; Maddie, M. A.; D'Souza, S. E.; Whittemore, S. R.; et al. Rescuing Vasculature with Intravenous Angiopoietin-1 and Alpha V Beta 3 Integrin Peptide Is Protective after Spinal Cord Injury. *Brain* **2010**, *133*, 1026–1042.
34. Prabhakar, U.; Maeda, H.; Jain, R. K.; Sevick-Muraca, E. M.; Zamboni, W.; Farokhzad, O. C.; Barry, S. T.; Gabizon, A.; Grodzinski, P.; Blakey, D. C. Challenges and Key Considerations of the Enhanced Permeability and Retention Effect for Nanomedicine Drug Delivery in Oncology. *Cancer Res.* **2013**, *73*, 2412–2417.
35. Peer, D.; Karp, J. M.; Hong, S.; Farokhzad, O. C.; Margalit, R.; Langer, R. Nanocarriers as an Emerging Platform for Cancer Therapy. *Nat. Nanotechnol.* **2007**, *2*, 751–760.
36. Davis, M. E. Nanoparticle Therapeutics: An Emerging Treatment Modality for Cancer. *Nat. Rev. Drug Discovery* **2008**, *7*, 771–782.
37. Papa, S.; Rossi, F.; Ferrari, R.; Mariani, A.; De Paola, M.; Caron, I.; Fiordaliso, F.; Bisighini, C.; Sammali, E.; Colombo, C.; et al. Selective Nanovector Mediated Treatment of Activated Proinflammatory Microglia/Macrophages in Spinal Cord Injury. *ACS Nano* **2013**, *7*, 9881–9895.
38. Wu, J.; Jiang, H.; Bi, Q.; Luo, Q.; Li, J.; Zhang, Y.; Chen, Z.; Li, C. Apamin-Mediated Actively Targeted Drug Delivery for Treatment of Spinal Cord Injury: More than Just a Concept. *Mol. Pharmaceutics* **2014**, *11*, 3210–3222.
39. Chvatal, S. A.; Kim, Y. T.; Bratt-Leal, A. M.; Lee, H. J.; Bellamkonda, R. V. Spatial Distribution and Acute Anti-inflammatory Effects of Methylprednisolone after Sustained Local Delivery to the Contused Spinal Cord. *Biomaterials* **2008**, *29*, 1967–1975.
40. Kim, Y. T.; Caldwell, J. M.; Bellamkonda, R. V. Nanoparticle-Mediated Local Delivery of Methylprednisolone after Spinal Cord Injury. *Biomaterials* **2009**, *30*, 2582–2590.
41. Sawyer, A. J.; Kyriakides, T. R. Nanoparticle-Based Evaluation of Blood-Brain Barrier Leakage during the Foreign Body Response. *J. Neural Eng.* **2013**, *10*, 016013.
42. Ishiyama, M.; Miyazono, Y.; Sasamoto, K.; Ohkura, Y.; Ueno, K. A Highly Water-Soluble Disulfonated Tetrazolium Salt as a Chromogenic Indicator for NADH as Well as Cell Viability. *Talanta* **1997**, *44*, 1299–1305.
43. Chung, I. Y.; Benveniste, E. N. Tumor Necrosis Factor-Alpha Production by Astrocytes: Induction by Lipopolysaccharide, IFN-Gamma, and IL-1-Beta. *J. Immunol.* **1990**, *144*, 2999–3007.
44. Stout, R. D.; Jiang, C. C.; Matta, B.; Tietzel, I.; Watkins, S. K.; Suttles, J. Macrophages Sequentially Change Their Functional Phenotype in Response to Changes in Microenvironmental Influences. *J. Immunol.* **2005**, *175*, 342–349.
45. Savaskan, N. E.; Fingerle-Rowson, G.; Buchfelder, M.; Eyüpoglu, I. Y. Brain Miffed by Macrophage Migration Inhibitory Factor. *Int. J. Cell Biol.* **2012**, 139573.
46. Miranda, K. M.; Espey, M. G.; Wink, D. A. A Rapid, Simple Spectrophotometric Method for Simultaneous Detection of Nitrate and Nitrite. *Nitric Oxide* **2001**, *5*, 62–71.
47. Scheff, S. W.; Rabchevsky, A. G.; Fugaccia, I.; Main, J. A.; Lumpp, J. E., Jr. Experimental Modeling of Spinal Cord Injury: Characterization of a Force-Defined Injury Device. *J. Neurotrauma* **2003**, *20*, 179–193.
48. Mukundan, S., Jr.; Ghaghada, K. B.; Badea, C. T.; Kao, C.-Y.; Hedlund, L. W.; Provenzale, J. M.; Johnson, G. A.; Chen, E.; Bellamkonda, R. V.; Annapragada, A. A Liposomal Nanoscale Contrast Agent for Preclinical CT in Mice. *Am. J. Roentgenol.* **2006**, *186*, 300–307.
49. Roller, B. T.; Munson, J. M.; Brahma, B.; Santangelo, P. J.; Pai, S. B.; Bellamkonda, R. V. Evans Blue Nanocarriers Visually Demarcate Margins of Invasive Gliomas. *Drug Delivery Trans. Res.* **2013**, 1–9.
50. Munson, J. M.; Fried, L.; Rowson, S. A.; Bonner, M. Y.; Karumbaiah, L.; Diaz, B.; Courtneidge, S. A.; Knaus, U. G.; Brat, D. J.; Arbiser, J. L.; et al. Anti-invasive Adjuvant Therapy with Imipramine Blue Enhances Chemotherapeutic Efficacy Against Glioma. *Sci. Transl. Med.* **2012**, *4*, 127ra36.
51. Butt, R. H.; Pfeifer, T. A.; Delaney, A.; Grigliatti, T. A.; Tetzlaff, W. G.; Coorssen, J. R. Enabling Coupled Quantitative Genomics and Proteomics Analyses from Rat Spinal Cord Samples. *Mol. Cell Proteomics* **2007**, *6*, 1574–1588.
52. Kroner, A.; Greenhalgh, A. D.; Zarruk, J. G.; Passos Dos Santos, R.; Gaestel, M.; David, S. TNF and Increased Intracellular Iron Alter Macrophage Polarization to a Detrimental M1 Phenotype in the Injured Spinal Cord. *Neuron* **2014**, *83*, 1098–1116.
53. Fenn, A. M.; Hall, J. C.; Gensel, J. C.; Popovich, P. G.; Godbout, J. P. IL-4 Signaling Drives a Unique Arginase+/IL-1beta+ Microglia Phenotype and Recruits Macrophages to the Inflammatory CNS: Consequences of Age-Related Deficits in IL-4Ralpha after Traumatic Spinal Cord Injury. *J. Neurosci.* **2014**, *34*, 8904–8917.
54. Bartus, K.; James, N. D.; Didangelos, A.; Bosch, K. D.; Verhaagen, J.; Yanez-Munoz, R. J.; Rogers, J. H.; Schneider, B. L.; Muir, E. M.; Bradbury, E. J. Large-Scale Chondroitin Sulfate Proteoglycan Digestion with Chondroitinase Gene Therapy Leads to Reduced Pathology and Modulates Macrophage Phenotype Following Spinal Cord Contusion Injury. *J. Neurosci.* **2014**, *34*, 4822–4836.
55. Mantovani, A.; Biswas, S. K.; Galdiero, M. R.; Sica, A.; Locati, M. Macrophage Plasticity and Polarization in Tissue Repair and Remodelling. *J. Pathol.* **2013**, *229*, 176–185.
56. David, S.; Kroner, A. Repertoire of Microglial and Macrophage Responses after Spinal Cord Injury. *Nat. Rev. Neurosci.* **2011**, *12*, 388–399.
57. Gilliver, S. C.; Emmerson, E.; Bernhagen, J.; Hardman, M. J. MIF: A Key Player in Cutaneous Biology and Wound Healing. *Exp. Dermatol.* **2011**, *20*, 1–6.
58. Popovich, P. G.; Horner, P. J.; Mullin, B. B.; Stokes, B. T. A Quantitative Spatial Analysis of the Blood Spinal Cord Barrier. 1: Permeability Changes after Experimental Spinal Contusion Injury. *Exp. Neurol.* **1996**, *142*, 258–275.
59. Saxena, T.; Karumbaiah, L.; Gaupp, E. A.; Patkar, R.; Patil, K.; Betancur, M.; Stanley, G. B.; Bellamkonda, R. V. The Impact of Chronic Blood-Brain Barrier Breach on Intracortical Electrode Function. *Biomaterials* **2013**, *34*, 4703–4713.
60. Bilgen, M.; Abbe, R.; Narayana, P. A. Dynamic Contrast-Enhanced MRI Of Experimental Spinal Cord Injury: *In Vivo* Serial Studies. *Magn. Reson. Med.* **2001**, *45*, 614–622.
61. Alexander, J. K.; Cox, G. M.; Tian, J.-B.; Zha, A. M.; Wei, P.; Kigerl, K. A.; Reddy, M. K.; Dagia, N. M.; Sielecki, T.; Zhu, M. X.; et al. Macrophage Migration Inhibitory Factor (MIF) Is Essential for Inflammatory and Neuropathic Pain and Enhances Pain in Response to Stress. *Exp. Neurol.* **2012**, *236*, 351–362.
62. Inácio, A. R.; Ruscher, K.; Leng, L.; Bucala, R.; Deierborg, T. Macrophage Migration Inhibitory Factor Promotes Cell

Death and Aggravates Neurologic Deficits after Experimental Stroke. *J. Cereb. Blood Flow Metab.* **2010**, *31*, 1093–1106.
63. Kithcart, A. P.; Cox, G. M.; Sielecki, T.; Short, A.; Pruitt, J.; Papenfuss, T.; Shawler, T.; Gienapp, I.; Satoskar, A. R.; Whitacre, C. C. A Small-Molecule Inhibitor of Macrophage Migration Inhibitory Factor for the Treatment of Inflammatory Disease. *FASEB J.* **2010**, *24*, 4459–4466.
64. Cox, G. M.; Kithcart, A. P.; Pitt, D.; Guan, Z.; Alexander, J.; Williams, J. L.; Shawler, T.; Dagia, N. M.; Popovich, P. G.; Satoskar, A. R. Macrophage Migration Inhibitory Factor Potentiates Autoimmune-Mediated Neuroinflammation. *J. Immunol.* **2013**, *191*, 1043–1054.
65. Noble, L. J.; Donovan, F.; Igarashi, T.; Goussev, S.; Werb, Z. Matrix Metalloproteinases Limit Functional Recovery after Spinal Cord Injury by Modulation of Early Vascular Events. *J. Neurosci.* **2002**, *22*, 7526–7535.
66. Kigerl, K. A.; Lai, W.; Rivest, S.; Hart, R. P.; Satoskar, A. R.; Popovich, P. G. Toll-like Receptor (TLR)-2 and TLR-4 Regulate Inflammation, Gliosis, and Myelin Sparing after Spinal Cord Injury. *J. Neurochem.* **2007**, *102*, 37–50.
67. Schmidt, J.; Metselaar, J. M.; Wauben, M. H.; Toyka, K. V.; Storm, G.; Gold, R. Drug Targeting by Long-Circulating Liposomal Glucocorticosteroids Increases Therapeutic Efficacy in a Model of Multiple Sclerosis. *Brain* **2003**, *126*, 1895–1904.
68. Stirling, D. P.; Cummins, K.; Mishra, M.; Teo, W.; Yong, V. W.; Stys, P. Toll-like Receptor 2-Mediated Alternative Activation of Microglia Is Protective after Spinal Cord Injury. *Brain* **2014**, *137*, 707–723.
69. Bastien, D.; Lacroix, S. Cytokine Pathways Regulating Glial and Leukocyte Function after Spinal Cord and Peripheral Nerve Injury. *Exp. Neurol.* **2014**, *258*, 62–77.
70. Bethea, J. R. Spinal Cord Injury-Induced Inflammation: A Dual-Edged Sword. *Prog. Brain Res.* **2000**, *128*, 33–42.
71. Klusman, I.; Schwab, M. E. Effects of Pro-inflammatory Cytokines in Experimental Spinal Cord Injury. *Brain Res.* **1997**, *762*, 173–184.
72. Shechter, R.; London, A.; Varol, C.; Raposo, C.; Cusimano, M.; Yovel, G.; Rolls, A.; Mack, M.; Pluchino, S.; Martino, G.; et al. Infiltrating Blood-Derived Macrophages Are Vital Cells Playing an Anti-inflammatory Role in Recovery from Spinal Cord Injury in Mice. *PLoS Med.* **2009**, *6*, e1000113.
73. Ferrante, C. J.; Pinhal-Enfield, G.; Elson, G.; Cronstein, B. N.; Hasko, G.; Outram, S.; Leibovich, S. J. The Adenosine-Dependent Angiogenic Switch of Macrophages to an M2-like Phenotype Is Independent of Interleukin-4 Receptor Alpha (IL-4Rα) Signaling. *Inflammation* **2013**, *36*, 921–931.
74. Bystrom, J.; Evans, I.; Newson, J.; Stables, M.; Toor, I.; van Rooijen, N.; Crawford, M.; Colville-Nash, P.; Farrow, S.; Gilroy, D. W. Resolution-Phase Macrophages Possess a Unique Inflammatory Phenotype That Is Controlled by cAMP. *Blood* **2008**, *112*, 4117–4127.
75. Shechter, R.; Miller, O.; Yovel, G.; Rosenzweig, N.; London, A.; Ruckh, J.; Kim, K.-W.; Klein, E.; Kalchenko, V.; Bendel, P.; et al. Recruitment of Beneficial M2Macrophages to Injured Spinal Cord Is Orchestrated by Remote Brain Choroid Plexus. *Immunity* **2013**, *38*, 555–569.
76. Miron, V. E.; Boyd, A.; Zhao, J.-W.; Yuen, T. J.; Ruckh, J. M.; Shadrach, J. L.; van Wijngaarden, P.; Wagers, A. J.; Williams, A.; Franklin, R. J.; et al. M2 Microglia and Macrophages Drive Oligodendrocyte Differentiation during CNS Remyelination. *Nat. Neurosci.* **2013**, *16*, 1211–1218.
77. Boutard, V.; Havouis, R.; Fouqueray, B.; Philippe, C.; Moulinoux, J. P.; Baud, L. Transforming Growth-Factor-Beta Stimulates Arginase Activity in Macrophages: Implications for the Regulation of Macrophage Cytotoxicity. *J. Immunol.* **1995**, *155*, 2077–2084.
78. Brancato, S. K.; Albina, J. E. Wound Macrophages as Key Regulators of Repair: Origin, Phenotype, and Function. *Am. J. Pathol.* **2011**, *178*, 19–25.
79. Martinez, F. O.; Gordon, S. The M1 and M2 Paradigm of Macrophage Activation: Time for Reassessment. *F1000Prime Rep.* **2014**, *6*, 13.
80. Tyor, W. R.; Avgeropoulos, N.; Ohlandt, G.; Hogan, E. L. Treatment of Spinal Cord Impact Injury in the Rat with Transforming Growth Factor-Beta. *J. Neurol. Sci.* **2002**, *200*, 33–41.
81. Lian, H.; Shim, D. J.; Gaddam, S. S. K.; Rodriguez-Rivera, J.; Bitner, B. R.; Pautler, R. G.; Robertson, C. S.; Zheng, H. IκB Alpha Deficiency in Brain Leads to Elevated Basal Neuroinflammation and Attenuated Response Following Traumatic Brain Injury: Implications for Functional Recovery. *Mol. Neurodegener.* **2012**, *7*, 47.
82. Plesnila, N.; von Baumgarten, L.; Retiounskaia, M.; Engel, D.; Ardeshiri, A.; Zimmermann, R.; Hoffmann, F.; Landshamer, S.; Wagner, E.; Culmsee, C. Delayed Neuronal Death after Brain Trauma Involves P53-Dependent Inhibition of NF-kappaB Transcriptional Activity. *Cell Death Differ.* **2007**, *14*, 1529–1541.
83. Mattson, M. P.; Meffert, M. K. Roles for NF-κB in Nerve Cell Survival, Plasticity, and Disease. *Cell Death Differ.* **2006**, *13*, 852–860.
84. Cho, M. L.; Moon, Y. M.; Heo, Y. J.; Woo, Y. J.; Ju, J. H.; Park, K. S.; Kim, S. I.; Park, S. H.; Kim, H. Y.; Min, J. K. NF-κB Inhibition Leads to Increased Synthesis and Secretion of MIF in Human CD4+ T Cells. *Immunol. Lett.* **2009**, *123*, 21–30.
85. Rothstein, J. D.; Jin, L.; Dykeshoberg, M.; Kuncl, R. W. Chronic Inhibition of Glutamate Uptake Produces a Model of Slow Neurotoxicity. *Proc. Natl. Acad. Sci. U.S.A.* **1993**, *90*, 6591–6595.
86. Papahadjopoulos, D.; Allen, T.; Gabizon, A.; Mayhew, E.; Matthay, K.; Huang, S.; Lee, K.; Woodle, M.; Lasic, D.; Redemann, C.; et al. Sterically Stabilized Liposomes: Improvements in Pharmacokinetics and Antitumor Therapeutic Efficacy. *Proc. Natl. Acad. Sci. U.S.A.* **1991**, *88*, 11460–11464.
87. Moghimi, S.; Szebeni, J. Stealth Liposomes and Long Circulating Nanoparticles: Critical Issues in Pharmacokinetics, Opsonization and Protein-Binding Properties. *Prog. Lipid Res.* **2003**, *42*, 463–478.
88. Saxena, T.; Gilbert, J.; Stelzner, D.; Hasenwinkel, J. Mechanical Characterization of the Injured Spinal Cord after Lateral Spinal Hemisection Injury in the Rat. *J. Neurotrauma* **2012**, *29*, 1747–1757.
89. Saxena, T.; Deng, B.; Stelzner, D.; Hasenwinkel, J.; Chaiken, J. Raman Spectroscopic Investigation of Spinal Cord Injury in a Rat Model. *J. Biomed. Opt.* **2011**, *16*, 027003.
90. Livak, K. J.; Schmittgen, T. D. Analysis of Relative Gene Expression Data Using Real-Time Quantitative PCR and the $2\Delta\Delta Ct$ Method. *Methods* **2001**, *25*, 402–408.
91. Collins, T. J. ImageJ for Microscopy. *Biotechniques* **2007**, *43*, 25–30.
92. Karumbaiah, L.; Norman, S. E.; Rajan, N. B.; Anand, S.; Saxena, T.; Betancur, M.; Patkar, R.; Bellamkonda, R. V. The Upregulation of Specific Interleukin (IL) Receptor Antagonists and Paradoxical Enhancement of Neuronal Apoptosis Due to Electrode Induced Strain and Brain Micromotion. *Biomaterials* **2012**, *33*, 5983–5996.
93. Weischenfeldt, J.; Porse, B. Bone Marrow-Derived Macrophages (BMM): Isolation and Applications. *CSH Protoc.* **2008**, 10.1101/pdb.prot5080.